Journal of Geophysical Research: Atmospheres

RESEARCH ARTICLE
10.1029/2018JD028697

Special Section:
The Arctic: An AGU Joint Special Collection

Modulation of Sea Ice Melt Onset and Retreat in the Laptev Sea by the Timing of Snow Retreat in the West Siberian Plain

Alex D. Crawford[1,2], **Sean Horvath**[1,3], **Julienne Stroeve**[1,4], **Rajagopalan Balaji**[3], and **Mark C. Serreze**[1]

[1]National Snow and Ice Data Center, Cooperative Institute for Research in Environmental Sciences, University of Colorado Boulder, Boulder, CO, USA, [2]Department of Earth Sciences, The College of Wooster, Wooster, OH, USA, [3]Department of Civil, Environmental and Architectural Engineering, University of Colorado Boulder, Boulder, CO, USA, [4]Earth Sciences Department, University College of London, London, UK

Abstract Recent years have seen growing interest in improving seasonal predictions of Arctic sea ice conditions, including the timing of ice melt onset and retreat, especially on the regional scale. This paper investigates potential links between regional sea ice melt onset and retreat in the southern Laptev Sea and retreat of terrestrial snow cover. Past studies have shown that variability of snow extent over Eurasia can substantially impact regional atmospheric circulation patterns over the North Pacific and Arctic Oceans. It is shown here that for the Laptev Sea, earlier melt onset and retreat of sea ice are encouraged by earlier retreat of snow cover over the West Siberian Plain. Earlier snow retreat in spring encourages greater ridging (e.g., at 500 hPa) over the East Siberian Sea through the summer. This results in more frequently southerly flow of warm, moist air over the Laptev Sea. This relationship could provide modest improvements to predictive skill for sea ice melt onset and retreat in the southern Laptev Sea at lead times of approximately 50 and 90 days, respectively. The detrended time series of snow retreat in the West Siberian Plain explains 26 and 29% of the detrended variance of the timing of sea ice melt onset and retreat in southern Laptev Sea, respectively.

Plain Language Summary Over the past several decades, decreasing in the amount of Arctic sea ice have allowed human activities, like shipping and tourism, to increase. Even though less sea ice exists in summer, plenty still forms in winter. Therefore, being able to forecast when the winter sea ice will disappear and Arctic waters will open up each summer is valuable to human activities. This study focuses on the Laptev Sea, which is part of the Northern Sea Route along the Russian Arctic coast. We show that by knowing when snow retreats from the West Siberian Plain, we can improve forecasts of when sea ice will retreat from the Laptev Sea later in the year. Especially valuable for forecasting, the snow retreat in the West Siberian Plain occurs about 90 days before the sea ice disappears in the Laptev Sea, so there is ample time to act on such forecasts. The physical link between these two regions is through the atmosphere. If snow melts away earlier than normal in the West Siberian Plain, the Laptev Sea experiences more winds blowing from south to north than normal. This brings more warm, wet air than normal, which helps melt the sea ice faster.

Key Points:
- Timing of sea ice melt onset and retreat in the Laptev Sea positively correlates with the timing of snow retreat in the West Siberian Plain
- Earlier snow retreat in the West Siberian Plain encourages southerly winds over the Laptev Sea, which promote earlier sea ice melt/retreat
- This relationship may aid seasonal sea ice forecasting, especially since the average lag between snow retreat and sea ice retreat is 93 days

Correspondence to:
A. D. Crawford,
acrawford@wooster.edu

Citation:
Crawford, A. D., Horvath, S., Stroeve, J., Balaji, R., & Serreze, M. C. (2018). Modulation of sea ice melt onset and retreat in the Laptev Sea by the timing of snow retreat in the West Siberian Plain. *Journal of Geophysical Research: Atmospheres*, *123*, 8691–8707. https://doi.org/10.1029/2018JD028697

Received 21 MAR 2018
Accepted 6 AUG 2018
Accepted article online 15 AUG 2018
Published online 29 AUG 2018

Author Contributions
Conceptualization: Alex D. Crawford, Julienne Stroeve
Data curation: Sean Horvath, Julienne Stroeve, Mark C. Serreze
Formal analysis: Alex D. Crawford, Sean Horvath, Rajagopalan Balaji
Funding acquisition: Julienne Stroeve, Rajagopalan Balaji, Mark C. Serreze
Investigation: Alex D. Crawford, Sean Horvath, Rajagopalan Balaji
Methodology: Alex D. Crawford, Julienne Stroeve, Rajagopalan Balaji, Mark C. Serreze
Resources: Sean Horvath, Julienne Stroeve, Rajagopalan Balaji, Mark C. Serreze
(continued)

1. Introduction

As the Arctic Ocean loses its summer sea ice cover, it becomes more accessible to marine shipping, extraction of natural resources, tourism, and other activities (e.g., Lahn & Emmerson, 2012). However, sea ice conditions will remain highly variable for decades to come, and variability may increase as the ice cover thins further (Holland & Stroeve, 2011). This drives a growing need for improved sea ice predictions (e.g., Stroeve et al., 2015). The question of when the Arctic Ocean will lose its summer sea ice cover has been widely addressed in the literature (Jahn et al., 2016; Notz & Stroeve, 2016; Overland & Wang, 2013; Stroeve et al., 2007; Stroeve, Kattsov, et al., 2012), and while this question has some applications to strategic planning, it is mainly of scientific interest. Stakeholders are more in need of information at the regional spatial scale and shorter time scales that can be used, for example, to plan for shipping activities and re-supply of ports. Prediction out to 7–10 days is possible through coupling an ice/ocean model to a numerical weather prediction model. For example, the U.S. Navy provides nowcasts up through seven-day forecasts of sea ice concentration (SIC), thickness, and motion via its Global Ocean Forecast System (GOFS 3.1; Metzger et al., 2014, 2017). At seasonal timescales (e.g., predicting when ice will retreat in a given area several months in advance), approaches range from the use of coupled models to statistical to heuristic approaches (Hamilton & Stroeve, 2016; Stroeve,

Supervision: Sean Horvath, Julienne Stroeve, Rajagopalan Balaji, Mark C. Serreze
Visualization: Alex D. Crawford
Writing - original draft: Alex D. Crawford, Sean Horvath, Rajagopalan Balaji, Mark C. Serreze
Writing – review & editing: Alex D. Crawford, Sean Horvath, Julienne Stroeve, Rajagopalan Balaji, Mark C. Serreze

Hamilton, et al., 2014). The Sea Ice Prediction Network (SIPN, https://www.arcus.org/sipn) provides a forum to compare the skill of seasonal predictions of both total and regional ice extent from different approaches.

Sea ice variability on both Arctic-wide and regional scales stems from oceanic and atmospheric forcing as well as sea ice preconditioning (e.g., ice thickness and melt pond distribution). With respect to oceanic forcing, heat inflows from the Pacific (Serreze et al., 2016; Woodgate et al., 2010; Woodgate et al., 2015) and the Atlantic (Schlichtholz, 2011) have been strongly implicated in driving ice anomalies in the Chukchi Sea and Nordic seas, respectively.

Responses to atmospheric variability involve both dynamic and thermodynamic components that often have reinforcing influences. Variations in the wind field can variously force offshore ice motion, resulting in regional reductions in ice extent or thickness (e.g., Rigor et al., 2002; Williams et al., 2016), or onshore motion, with the opposite effect. Thermodynamic influences involve processes that affect surface energy exchanges. For example, winds from the south that advect ice offshore also tend to be warm winds that can limit winter ice growth or hasten summer melt (Mortin et al., 2016). Anomalies in temperature and snow cover on sea ice can affect summer melt pond coverage, influencing albedo and hence summer melt rates (Schröder et al., 2014).

Given the recognized importance of summer melt ponds and albedo, recent work has focused on the timing of seasonal melt onset. If melt onset is early, this means an earlier drop in the surface albedo, favoring earlier development of melt ponds and exposure of dark open water which hastens further melt, and increases the internal energy of the ocean mixed layer. This in turn delays autumn freezeup (Serreze et al., 2016; Stammerjohn et al., 2012; Stroeve, Serreze, et al., 2012; Stroeve et al., 2016). Melt onset in turn appears to be strongly tied to the influx of warm and moist air masses over the ice cover (often but not necessarily associated with low-level Arctic stratus) that increases the flux of longwave radiation to the surface (Kapsch et al., 2013, 2016; Liu & Schweiger, 2017; Mortin et al., 2016).

The present paper addresses connections between the timing of terrestrial snow cover retreat and the timing of sea ice melt onset and ice retreat in the southern Laptev Sea (SLS; Figure 1), which lies along the Northern Sea Route. Of any region in the Arctic Ocean, the Laptev Sea demonstrates the greatest potential for enhancing seasonal predictions via the timing of snow retreat (Figure S1). One possible link is between snow cover and local/regional temperature and humidity anomalies: an early removal of snow along the coast could result in early warming and moistening of the overlying atmosphere, leading to earlier sea ice melt onset and retreat downwind of the snow cover anomaly. Another possibility is that early removal of snow modifies regional atmospheric circulation patterns, with both dynamic and thermodynamic influences on the ice cover.

Based on past research, both mechanisms are plausible. While results from some studies (e.g., Kumar & Yang, 2003; Peings et al., 2011) point to only low-level impacts on the atmosphere from snow cover anomalies, others point to robust influences on atmospheric circulation. Clark and Serreze (2000) observe that an extensive East Asian snow cover is associated with a deeper Aleutian Low and lower temperatures downwind; Orsolini and Kvamstø (2009) arrive at similar conclusions. García-Herrera and Barriopedro (2006) suggest that regional snow cover anomalies over the continents can modulate atmospheric blocking patterns over adjacent (to the east) oceans. Gong et al. (2007) find that snow anomalies in northern Eurasia are better able to influence circulation patterns than snow anomalies in other regions because (a) Northern Eurasia's large size allows for great variability in snow extent, (b) it extends over appropriate latitudes for substantial snow variability, and (c) Northern Eurasia is an area of great stationary wave activity (in part because of its isolation from other land areas by orographic barriers). The last aspect is important because it allows snow anomalies to propagate (vertically and horizontally). Similarly, Xu and Dirmeyer (2011) find that coupling between the atmosphere and snow cover variability is strongest during the snowmelt period when the albedo feedback mechanism operates. They also emphasize that the *snow transition zone* (about 40 to 70°N) is the only important area for snow albedo effects because it (a) has enough snow and (b) receives sufficient shortwave radiation. Note, though, that they focus only on local effects of snowmelt on atmospheric conditions.

Focusing on remote effects, Matsumura et al. (2010) describe land-atmosphere coupling in western Siberia, whereby lower springtime snow cover leads to a warmer surface and amplified Rossby wave activity. This activity then propagates eastward throughout the summer (Matsumura et al., 2010; Matsumura &

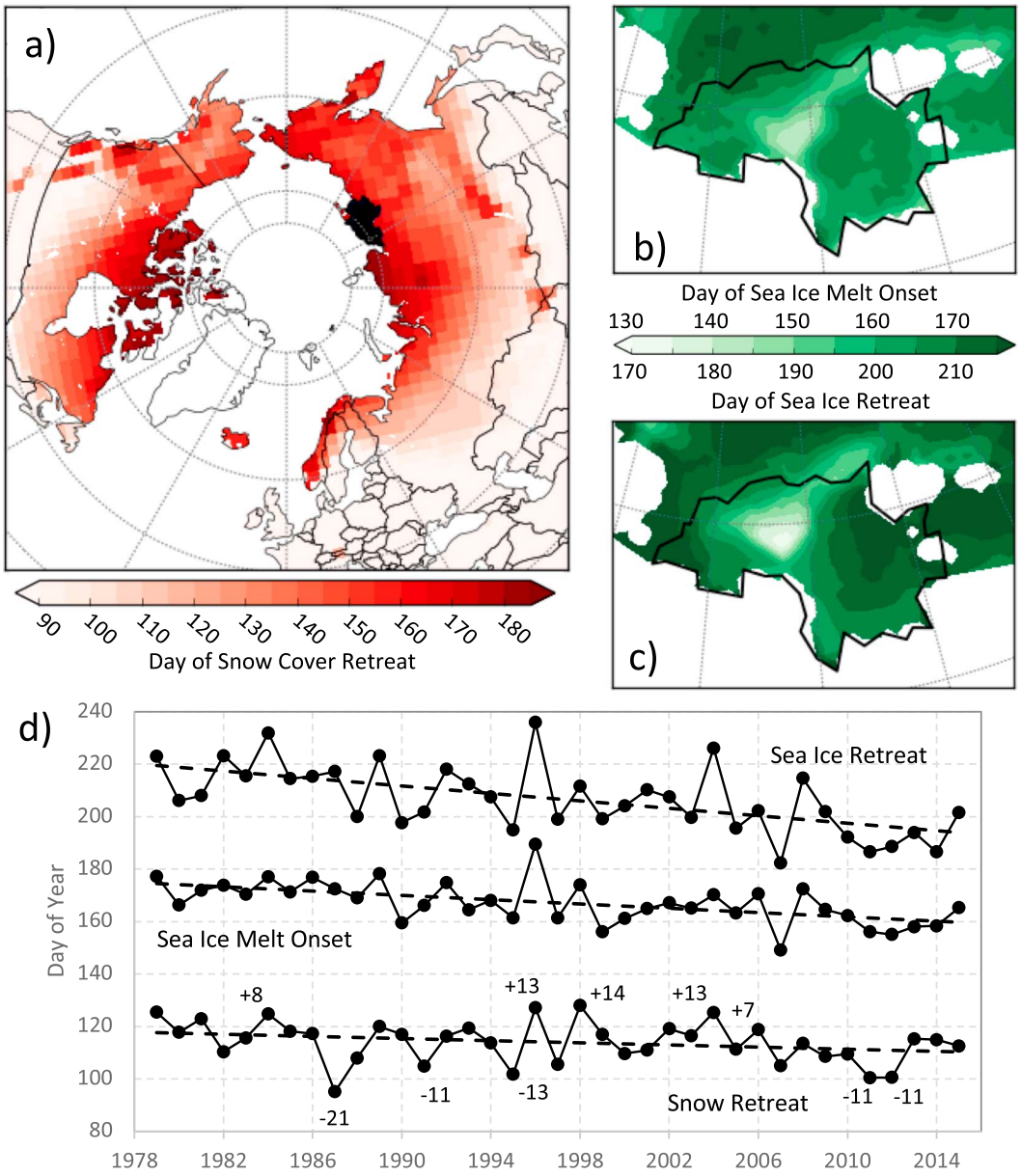

Figure 1. Climatology (1979–2015) of (a) terrestrial snow retreat day and (b) sea ice melt onset and (c) retreat in the Laptev Sea. The location of the southern Laptev Sea (black) is defined by the smoothed outline of grid cells in the Laptev Sea for which sea ice concentration falls below 15% during at least 35 years. (d) Time series of snow retreat day in the West Siberian Plain and sea ice melt onset and retreat days in the Laptev Sea (solid lines) and their linear trends (dotted lines). Detrended values of snow retreat day in the 10 years used for composite analysis are indicated.

Yamazaki, 2012). Similarly, Matsumura et al. (2014) describe how earlier snowmelt over Eurasia enhances rising motion over the land, and compensating subsidence and adiabatic warming in the Arctic troposphere, favoring a negative phase of the summer Arctic Oscillation (AO). This is manifest as positive sea level pressure (SLP) anomalies over the central Arctic Ocean—a pattern conducive to summer sea ice export through Fram Strait (Ogi & Wallace, 2007).

In this study, we examine the potential role of terrestrial snow cover anomalies on sea ice melt onset and retreat in the SLS using available records of sea ice and snow along with output from version 2 of the Modern-Era Retrospective Analysis for Research and Applications (MERRA2). Section 2 provides an overview of the data and methods. Results presented in section 3 are organized around three questions:

1. Are there regions for which terrestrial snow cover variability correlates with sea ice melt onset and retreat in the SLS?
2. What is the physical basis for the West Siberian Plain (WSP)-Laptev Sea connection?
3. What is the potential for this relationship to improve seasonal predictions of sea ice melt onset and retreat in the SLS?

Results addressing the first question demonstrate a strong statistical link between variability of sea ice melt onset and retreat in the SLS and variability in snow retreat over the WSP, so this connection becomes the focus for the final two research questions. Implications for seasonal sea ice predictability, comparison to past work, and limits to our interpretation are discussed in section 4.

2. Data and Methods

2.1. Sea Ice and Snow Cover

For SIC, we use the combined record at 25-km resolution from the Nimbus Scanning Multichannel Microwave Radiometer (SMMR, 1979–1987), the Defense Meteorological Satellite Program (DMSP) Special Sensor Microwave/Imager (SSM/I, 1987–2007), and the Special Sensor Microwave Imager/Sounder (SSMIS, 2007–2015). The record uses the National Aeronautics and Space Administration (NASA) Team sea ice algorithm (Cavalieri et al., 1996) and is distributed by the National Snow and Ice Data Center (NSIDC; http://nsidc.org/data/NSIDC-0051). The sea ice retreat day is calculated following the approach of Stroeve et al. (2016). Briefly, for each year at each sea ice grid cell, a 5-point moving average is applied to the daily SIC time series. This reduces variability from short-term ice dynamics. Next, the day of minimum SIC is identified. For each year, the last time SIC falls below 15% before the minimum is reached is defined as the last retreat day. If a grid cell never experiences retreat, it is labeled as *not a number* for that year.

The combined passive microwave record is also used to determine the onset of continuous sea ice melt (Markus et al., 2009; Stroeve, Markus, et al., 2014; https://neptune.gsfc.nasa.gov/csb/index.php?section=54). This method takes advantage of how the amount of liquid water at the surface influences brightness temperatures at 19 and 37 GHz. The addition of meltwater at the surface increases ice and snow emissivity to near 1 at microwave wavelengths (Markus et al., 2009), allowing for detection of the onset of continuous melt.

For snow cover, we use the weekly National Oceanic and Atmospheric Administration/National Climatic Data Center (NOAA/NCDC) Climate Data Record (CDR) of Northern Hemisphere (NH) snow cover extent product (Robinson, 2012). This product is derived from manual interpretation of visible satellite data, including Geostationary Operational Environmental Satellite (GOES) and Advanced Very High Resolution Radiometer (AVHRR; Helfrich et al., 2007). The version available at NSIDC (http://nsidc.org/data/NSIDC-0046) has been regridded to version 2 of the Equal-Area Scalable Earth (EASE2) Grid with a 25-km spatial resolution (Brodzik & Armstrong, 2013). The snow cover retreat day is determined by the first week with snow-free conditions. Since the data are weekly, the first day for each weekly file is used as the retreat day.

2.2. Correlation Between Snow and Sea Ice Events

Before comparing these three time series (snow retreat, sea ice melt onset, and sea ice retreat), the data were detrended for the 1979–2015 period at all valid grid cells (those with at least 35 years for which concentration fell below 15%). Concentration at some grid cells in the northern Laptev Sea region rarely or never declined below 15% concentration in the 1980s but did at the end of the record. Therefore, all spatial averaging is limited to grid cells in the SLS (Figure 1).

To identify land regions where snow retreat is a potential predictor of ice melt onset and retreat in the SLS, the detrended snow retreat time series at each NH grid cell was compared to the regional average time series of ice melt and retreat for the SLS using Pearson's r and mutual information. Although a correlation coefficient is more easily interpretable, mutual information is useful for comparing time series because it is nonparametric and can capture nonlinear relationships. It is used here as an additional check on the linear relationships being explored. Mutual information was calculated using kernel density estimators, following Moon et al. (1995). Confidence intervals of the resulting scores were determined using a 500-sample Monte Carlo simulation. The WSP was identified as a region of interest for predicting sea ice melt onset and retreat in the SLS because it is the largest area of contiguous grid cells for which both the Pearson's r and mutual information score are significant at a 90% confidence interval.

2.3. Examining the Atmospheric Pathway

The method just described allowed us to identify a statistical connection between snow retreat in the WSP and sea ice melt/retreat in the SLS. To examine the physical mechanisms underlying this connection, we examined a series of atmospheric variables from MERRA2 (Gelaro et al., 2017; https://disc.sci.gsfc.nasa.gov/daac-bin/FTPSubset2.pl? LOOKUPID_List=M2T1NXSLV). This atmospheric reanalysis uses the Goddard Earth Observing System, Version 5.12.4 (GEOS-5) atmospheric model and Global Statistical Interpolation (GSI) analysis scheme. Updates from the original MERRA effort include the assimilation of aerosol observations, seasonally variable sea ice albedo, and several improvements that reduce biases in the water cycle (ibid.). MERRA2 has an approximate spatial resolution of 0.5° latitude by 0.625° longitude and 72 hybrid-eta levels from the surface to 0.01 hPa. Matching the temporal resolution of the sea ice data set, daily SLP, geopotential height (GPH) at 500 hPa, total column water vapor, downwelling longwave and shortwave radiation at the surface, surface sensible and latent heat fluxes, temperature from 1,000 to 100 hPa, and zonal, meridional, and vertical wind components from 1,000 to 100 hPa were obtained for the period 1980–2015. The monthly AO Index (Thompson & Wallace, 1998) was obtained from NOAA (http://www.cpc.ncep.noaa.gov/products/precip/CWlink/daily_ao_index/ao.shtml).

Three frameworks were used to compare pathways. First, atmospheric variables were composited for the most extreme pentads of detrended WSP snow retreat. The pentad of 1984, 1996, 1998, 2004, and 2006 had extremely late snow retreat, and the pentad of 1987, 1991, 1995, 2011, and 2012 had extremely early retreat (Figure 1d). Composites were calculated for three 30-day periods: 10 April to9 May, 2 June to 1 July, and 12 July to 10 August. These periods are centered on the average day of snow retreat in the WSP, sea ice melt onset in the SLS, and ice retreat in the SLS, respectively. Because of significant long-term trends in temperature and downwelling longwave radiation, the time series of these variables were also detrended. The difference of composite means was tested with a Wilcoxon test. As a further diagnostic tool, the Eliassen-Palm (EP) flux was calculated throughout the atmospheric column following the method of Edmon Jr. et al. (1980) (temperatures not detrended). In cross section, EP flux vectors directed upward from the surface indicate Rossby wave generation. The horizontal wave activity flux at 500 hPa was calculated from GPH and horizontal wind components following the method of Takaya and Nakamura (2001) after applying an eight-day low-pass filter. Resulting vectors indicate the direction of Rossby wave propagation. For all composites, the hypothesis is that if an atmospheric link between WSP snow retreat and sea ice melt onset/retreat in the SLS exists, then the composite analyses will show contrasting atmospheric conditions for early snow retreat and late snow retreat years.

For the second framework of comparison, all atmospheric variables were regionalized for the SLS region for the same three periods described above, and Pearson's *r* correlations were computed between these regional time series and the WSP snow retreat time series. If snow retreat in the WSP has a physical influence on sea ice melt onset/retreat in the SLS through an atmospheric pathway, then a significant correlation with atmospheric variables over the SLS is expected for the 2 June to1 July and 12 July to 10 August periods but not the 10 April to 9 May period.

2.4. Back Trajectories

Whereas the first two frameworks consider how variation in WSP snow retreat links to atmospheric conditions in subsequent periods, the third framework considers whether variations in sea ice melt onset/retreat in the SLS are preceded by particular variations in atmospheric circulation. Back trajectories provide insight into the origin and pathway of air particles and their physical characteristics. The approach has commonly been used in air pollution modeling but has also been useful in moisture source identification (Bracken et al., 2015; Gustafsson et al., 2010; Wegmann et al., 2015). We are interested in back trajectories that document the advection of warm, moist air to the SLS for the period leading up to melt onset/retreat. For each year of study, back trajectories were created using the Hybrid Single-Particle Lagrangian Integrated Trajectory (HYSPLIT, version 4; Draxler, 1999; Draxler & Hess, 1997, 1998). Eight-day, 3-D kinematic back trajectories were computed for arrival times of 0:00UTC, 6:00UTC, 12:00UTC, and 18:00UTC each day from 9 May (the end of the snow retreat period) to the day of ice melt/retreat, and originating at two heights, 10 m and 925 hPa. Climate data were obtained from the National Centers for Environmental Prediction/National Center for Atmospheric Research (NCEP/NCAR) Global Reanalysis (Kalnay et al., 1996), accessed through the HYSPLIT Graphical User Interface (GUI).

Clustering for each altitude was done independently using the Trajectory Cluster Analysis tool of HYSPLIT (Draxler et al., 2016). This employs a method of k-means clustering where the spatial variance (SV) is computed for each endpoint (k) along trajectory (j) within its cluster (i):

$$SV_{i,j} = \Sigma\left(P_{j,k} - M_{i,k}\right)^2 \tag{1}$$

where **P** and **M** are position vectors for the individual trajectory and its cluster mean trajectory, respectively.

The cluster spatial variance(CSV), which is the sum of the SV of all trajectories within its cluster, is then calculated as

$$\mathrm{CSV}_i = \Sigma \mathrm{SV}_{i,j} \tag{2}$$

and the total spatial variance (TSV) is found by

$$\mathrm{TSV} = \Sigma \mathrm{CSV}_{j,k} \tag{3}$$

This algorithm starts with each trajectory as its own cluster. In each iteration, two clusters are merged together, reducing the total number of clusters by one, and the TSV is calculated. The optimum number of clusters is found by observing when the TSV rises dramatically near the end of the computation.

2.5. Seasonal Predictability of Sea Ice Melt Onset and Ice Retreat

To further assess the utility of snow cover retreat in the WSP as a predictor of sea ice melt onset and retreat in the SLS, linear regression models using snow retreat as the predictor were compared to other possible combinations of right-hand variables:

1. Detrended SIC in the SLS on 9 May, which is the end of the snow retreat period and postdates the latest WSP snow retreat for the full time series. This is similar to an anomaly persistence model.
2. WSP snow retreat day and SIC on 9 May.
3. Every possible combination of 12 atmospheric variables averaged over the SLS for the period 10 April to 9 May, where the possible variables are temperature at 2 m or 925 hPa, temperature advection at 925 hPa, total column water vapor, downwelling longwave radiation, downwelling shortwave radiation, sensible heat flux, latent heat flux, SLP, zonal and meridional wind at 925 hPa, and 500 hPa GPH.
4. Every possible combination of all atmospheric variables plus WSP snow retreat day and SIC on 9 May.

Given that this method yields over 32,000 models, results reported from options 3 and 4 above are both limited to the model with the lowest Bayesian Information Criterion (BIC; Schwarz, 1978).

$$\mathrm{BIC} = \ln(n)k - 2\ln\left(\widehat{L}\right) \tag{4}$$

BIC is a measure that comprises model fit (the maximum likelihood function $\widehat{L}$), the number of observations (n), and model size (k). Lower BIC is considered better, and adding additional parameters increases BIC.

3. Results

3.1. Correlations

Detrended time series of sea ice melt onset and retreat for the SLS were compared to detrended snow retreat time series for every terrestrial grid cell in the NH (Figure 2). Using either Pearson's r or a mutual information criterion, sea ice melt onset in the SLS has a significant relationship with snow retreat throughout much of central and western Siberia and no connection to snow retreat in Europe, east Asia, or North America. Significant connections to sea ice retreat are more restricted. Both criteria are significant only in a narrow swath roughly corresponding to the WSP. This relationship is robust to outliers and time series divisions, such as if 1979–1997 and 1998–2015 are considered separately (not shown).

Given that melt onset and retreat in the SLS exhibit a robust, significant statistical connection to a single, contiguous region for all tests, the remainder of the results in this study focuses on the WSP for snow retreat.

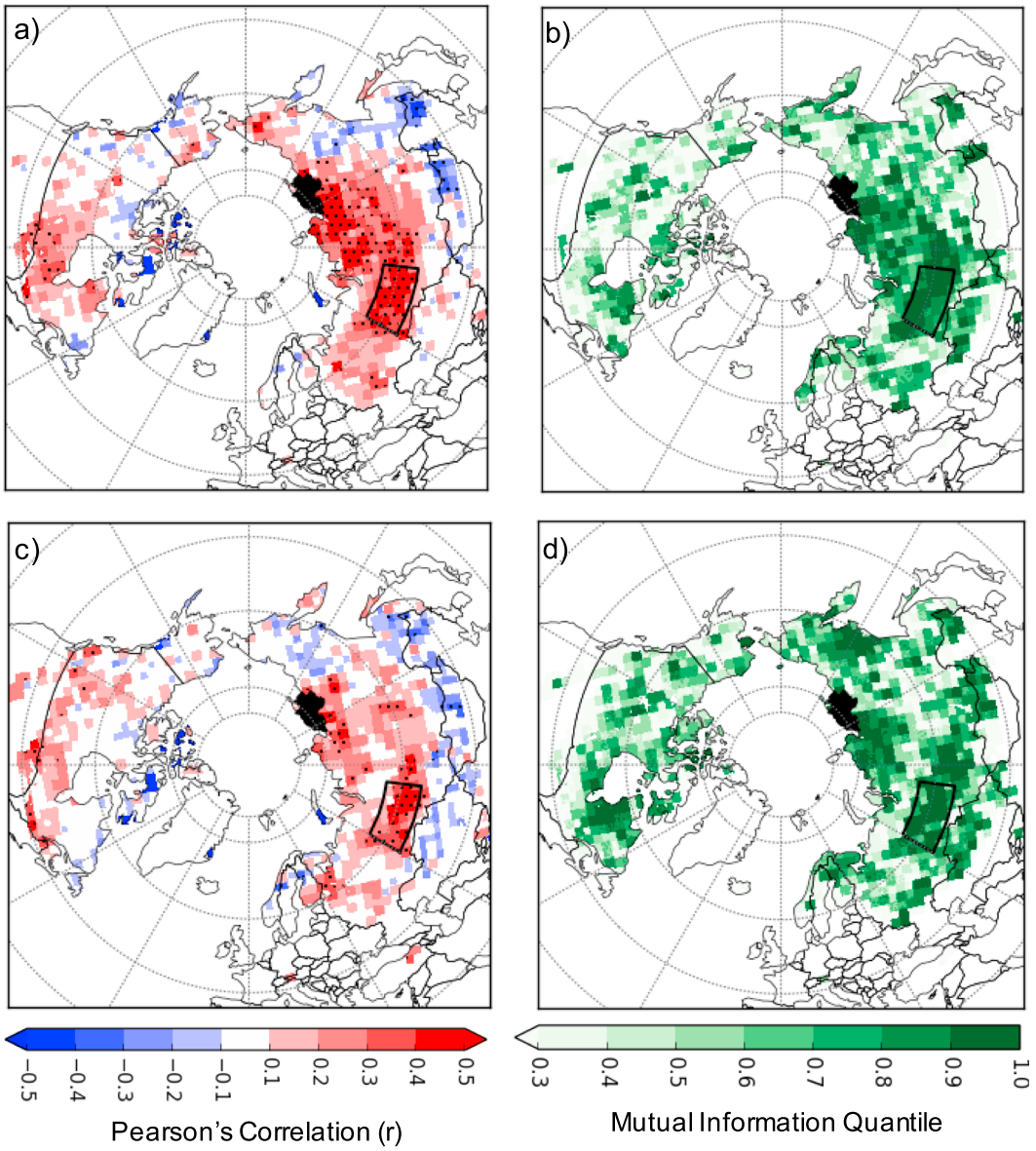

Figure 2. Comparison of the timing of (a and b) sea ice melt onset and (c and d) retreat in the southern Laptev Sea (black shading) to the timing of snow cover retreat throughout the Northern Hemisphere using Pearson's *r* (a and c) and a mutual information criterion (b and d). Pearson's correlations for which the *p*-value <0.1 are indicated by stippling. The region of common significant relationships for all four plots in the West Siberian Plain is outlined in black.

More specifically, the area used for spatial averaging (outlined in Figures 1a and 2) is the largest area of contiguous grid cells for which *both* Pearson's *r* and the mutual information criteria yield a significant relationship with sea ice retreat. This results in a more restrictive region than using sea ice melt onset. Comparing region to region (Table 1), snow cover in the WSP typically retreats on 24 April ± 8 days. Sea ice melt onset in the SLS occurs about 7.5 weeks later, on 16 June ± 8 days. Sea ice retreat in the SLS is another 7 weeks later, and the timing is more variable: 26 July ± 13 days. In total, the time lag between snow retreat and sea ice retreat is 93 days, but the correlation is 0.54, about the same as the correlation between snow retreat and sea ice melt onset. The positive correlation indicates that when snow cover disappears earlier than normal in the WSP, sea ice in the SLS typically experiences earlier melt onset and earlier retreat.

Table 1
Relationship Between Snow Cover Retreat in the West Siberian Plain and Sea Ice Melt Onset and Retreat in the Southern Laptev Sea

	μ (date/day of year)	σ (days)	Mutual information quantile	*r* (*p*-value)
West Siberian Plain Snow Retreat	24 April (114)	7.8	–	–
Laptev Sea Ice Melt Onset	16 June (167)	7.8	0.97	0.51 (0.0012)
Laptev Sea Ice Retreat to 15%	26 July (207)	12.8	0.98	0.54 (0.0006)

Note. All time series are detrended before comparison.

3.2. Atmospheric Pathways

Results from section 3.1 show that a positive correlation exists between snow retreat in the WSP and both melt onset and retreat of sea ice in the SLS, but what physical mechanisms might explain this connection? Several methods were used to test whether an atmospheric pathway exists that could connect these events. As a first test, atmospheric conditions were composited for the five years with the earliest and latest detrended WSP snow retreat. Composites (Figures S3–S10) were calculated for three periods centered on the average timing of the three events: 10 April to 9 May (the snow retreat period), 2 June to 1 July (the sea ice melt onset period), and 12 July to 10 August (the sea ice retreat period). The composite differences between early snow retreat years and late snow retreat years are shown in Figures 3 and 4.

Looking first at the snow retreat period, early WSP snow retreat is associated with anomalous ridging at 500 hPa (Figure 3a) and lower pressure heights than normal over the Arctic Ocean. Near-surface winds blowing into the WSP are more southerly than normal, and air is warmer and wetter (Figures 3d, 3g, and 3j). These parameters, along with greater downwelling radiation (Figure 4a**)**, may all contribute to the earlier retreat. Conversely, greater sensible and latent heat fluxes to the atmosphere in the WSP are likely part of the response to losing the snow cover (Figures 4g and 4j). In the SLS, on the other hand, moisture content and downwelling longwave radiation are only slightly greater in early snow retreat years than the late snow retreat years. Other variables show no significant change.

After especially late WSP snow retreat, a relatively strong polar vortex develops in June, reminiscent of a positive AO, but with a center over the Taymyr Peninsula rather than the central Arctic Ocean (Figure S3). By contrast, 500-hPa heights are higher over much of the Arctic when snow retreat is especially early, and a ridge forms over the East Siberian and Chukchi Seas. In the composite difference (Figure 3b), this means that when WSP snow retreat is much earlier than normal, anomalously low 500-hPa heights lie to the southwest of the Laptev Sea and anomalously high 500-hPa heights lie to the north. This difference helps drive southeasterly wind anomalies into the SLS (Figure 3k) and therefore warmer, wetter conditions (Figures 3e and 3h). Cloudier conditions over the SLS in early snow retreat years are also indicated by more downwelling longwave radiation and less downwelling shortwave radiation (Figures 4b and 4e). By contrast, June has little local difference (over the WSP) in the atmospheric state between years with early and late snow retreat. The atmosphere is drier in June following especially early retreat, but otherwise the two composites are similar.

The circulation differences apparent during the ice melt period become magnified over the following weeks. From 12 July to 10 August, the average polar vortex position is centered over the North Pole in years following late WSP snow retreat (Figure S3). The vortex is weaker and shifted toward the Atlantic side of the Arctic Ocean when snow retreat is especially early. This sets up a distinct dipole in the composite difference (Figure 3c). When snow retreats early, 500-hPa heights are greater over the Kolyma Lowland and East Siberian Sea and lower over the Kara Sea and Taymyr Peninsula. The SLS itself lies in between these two centers of action, but its position downstream of a trough in the 500-hPa height field means southerly wind anomalies and warmer, wetter conditions near the surface (Figures 3f, 3i, and 3l). However, temperature advection is not significantly different between the composites for this period, suggesting that continued temperature differences are driven more by moisture advection and enhanced downwelling longwave radiation (Figure 4c).

One way to visualize the translation from snow anomalies to circulation anomalies is through the EP flux, which was calculated for the limited zone of 60–80°E during 10 April to 9 May. As with other variables, a composite difference between early and late snow retreat years was performed (Figure 5). Upward-pointing

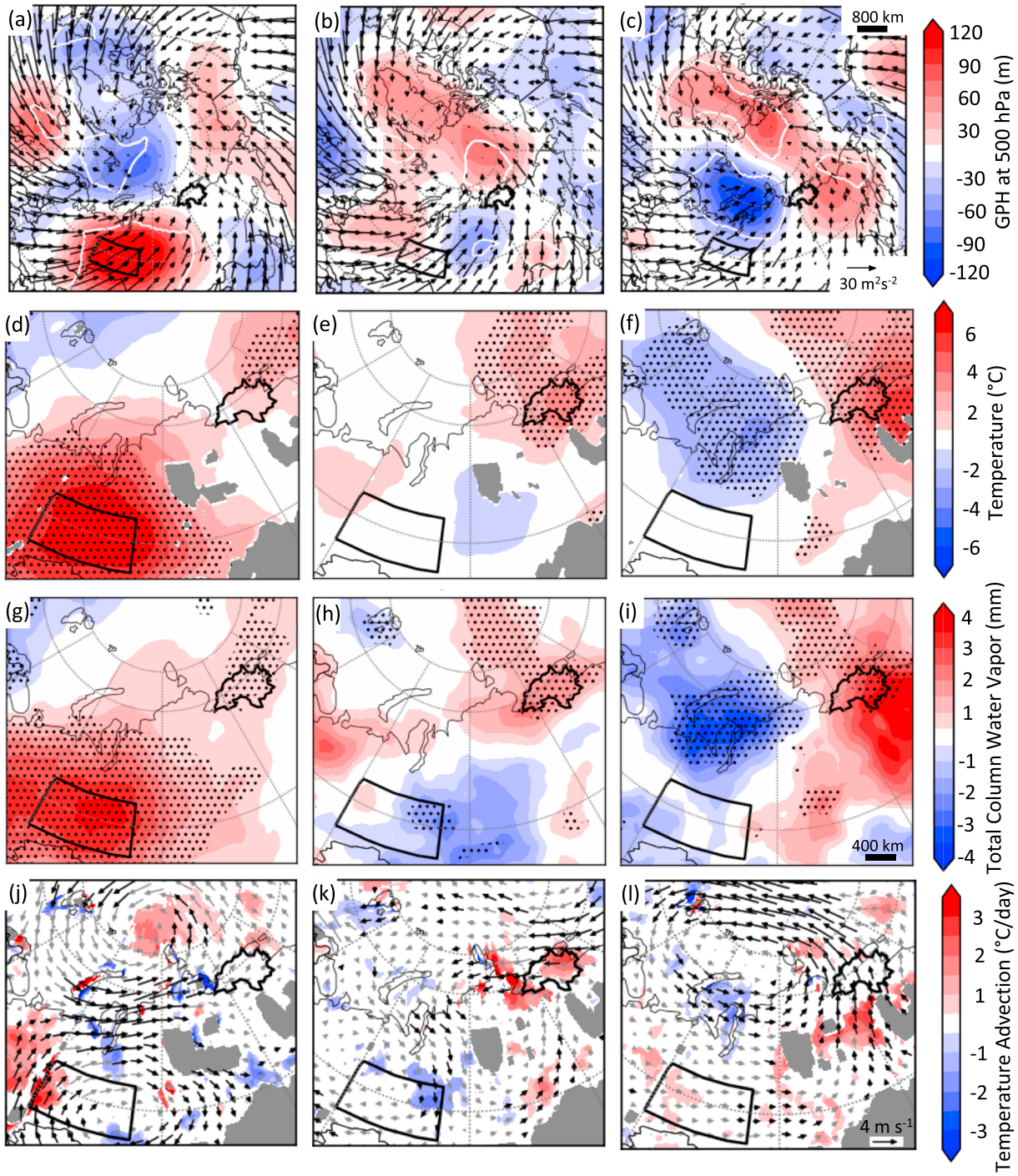

Figure 3. Composite differences of years with extreme early snow retreat minus years with extreme late snow retreat in the West Siberian Plain for three periods: (left) 10 April to 9 May, (middle) 2 June to 1 July, and (right) 12 July to 10 August. Composites are of geopotential height (GPH) at (a–c) 500 hPa, (d–f) temperature at 925 hPa, (g–i) total column water vapor, and (j–l) temperature advection at 925 hPa with wind vectors. Because of significant trends in the time series, temperature and downwelling longwave radiation were detrended before compositing. Significant differences ($p < 0.10$) are noted by white contours in a–c, stippling in d–i, and black vectors in j–l. To reduce clutter, temperature advection is only plotted when significant. The average horizontal wave activity flux at 500 hPa is overlain on a–c.

vectors show enhanced wave activity over the latitude of the WSP when snow retreat is especially early. Convergence (blue shading) in the upper troposphere demonstrates deceleration of the westerly jet. This response is a strictly regional phenomenon; calculating the EP flux for the average of all longitudes yields no notable differences for early and late snow retreat years (not shown). Note that this translation from

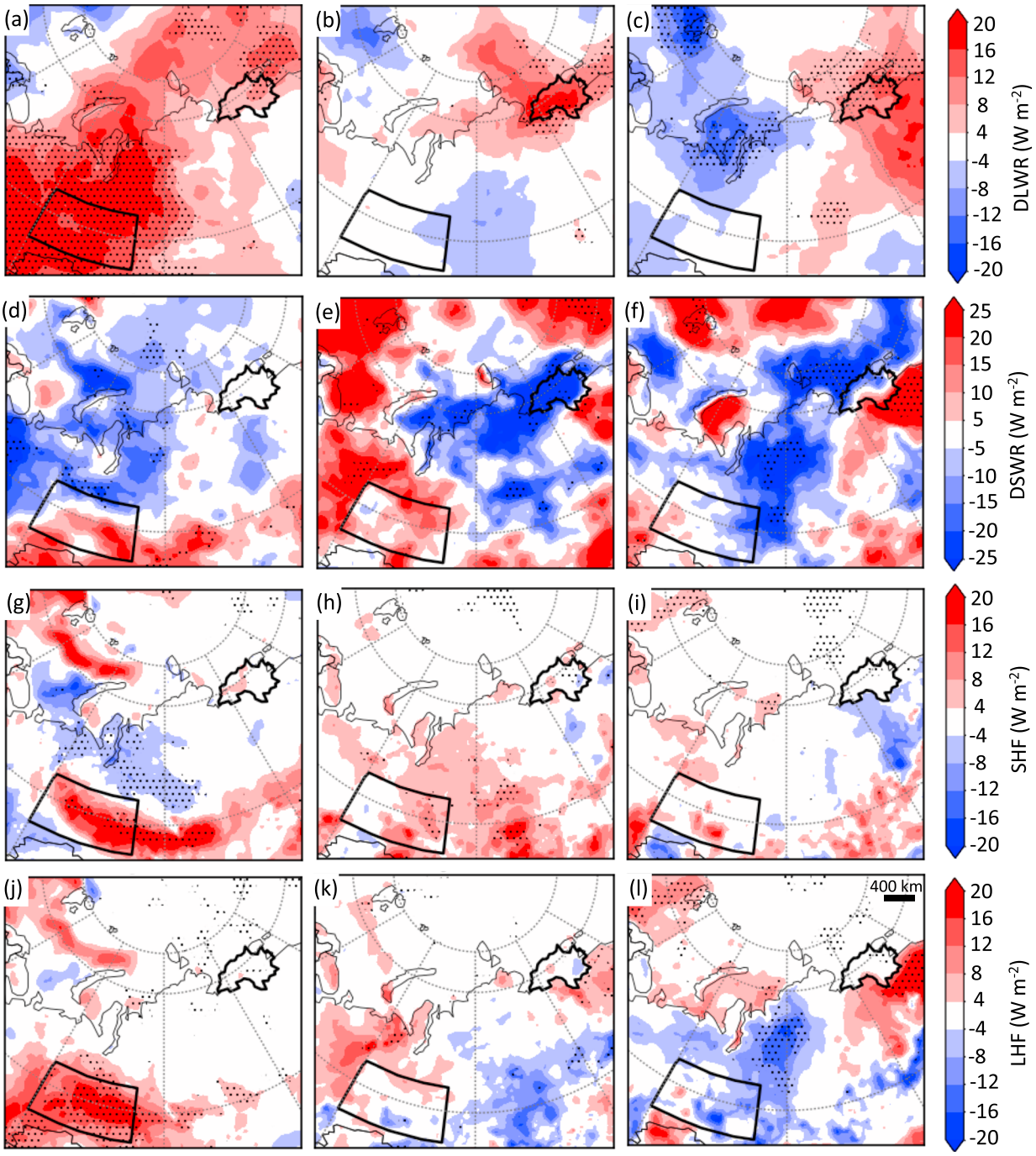

Figure 4. Composite differences of years with extreme early snow retreat minus years with extreme late snow retreat in the West Siberian Plain for three periods: (left) 10 April to 9 May, (middle) 2 June to 1 July, and (right) 12 July to 10 August. Composites are of (a–c) downwelling longwave radiation (DLWR), (d–f) downwelling shortwave radiation (DSWR), (g–i) upward sensible heat flux (SHF), and (j–l) upward latent heat flux (LHF). Stippling denotes a significant difference ($p < 0.10$).

surface of the WSP to atmosphere occurs during the snow retreat period, but these waves then propagate eastward from early June to mid-August (Figures 3a–3c).

We also tested the presence of a physical link between WSP snow retreat and SLS ice melt/retreat using regional correlations (Table 2). The detrended snow retreat time series was compared to the time series of atmospheric parameters that were spatially averaged over the SLS (Figure 1) and temporally averaged for the three periods of interest. The only atmospheric variable with a significant relationship with WSP snow

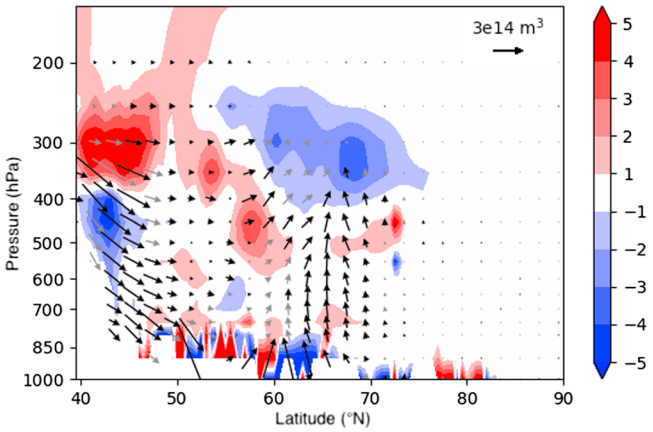

Figure 5. Composite differences of both the Eliassen-Palm flux and its divergence calculated as years with extreme early snow retreat minus years with extreme late snow retreat in the West Siberian Plain for the period 10 April to 9 May. Zonal averaging for the input parameters of the Eliassen-Palm flux was conducted for the longitudes 60° to 80°, coinciding with the zonal extent of the West Siberian Plain study area. The vectors and divergence are scaled for display following the method of Edmon Jr. et al. (1980). Units are 1e14 m^3 for vectors, and the contour interval is 1e15 m^3 for divergence. The colored regions and vectors plotted in black are significant ($p < 0.10$).

retreat during the snow retreat period is water vapor, although that correlation would not be significant using a stricter 95% confidence level.

In contrast, when comparing the same variables during the ice melt period (i.e., averaging for the period 2 June to 1 July), significant correlations abound. Negative values indicate that when snow retreat is earlier in the WSP, June winds are more often southerly over the SLS, the air is warmer and (somewhat) wetter, and downwelling longwave radiation is greater although downwelling shortwave radiation is lesser. This in turn leads to earlier melt onset (Table 1). Considering the SLS atmosphere during the period when the ice is retreating (from 12 July to 10 August), the same patterns hold as for 2 June to 1 July, only the magnitude of the correlation for most variables increases. As in Figures 3 and 4, warmer and wetter air leads to earlier ice retreat (Table 1), but temperature advection is no longer significantly correlated snow retreat.

Finally, our third framework for assessing the connection between snow retreat in the WSP and sea ice melt and retreat in the SLS involved the clustering of a series of eight-day back trajectories. Multiple source points and levels were assessed, each yielding similar results. Figure 6 is limited to a representative example of the 925-hPa level and a source of 73°N, 135°E. In all cases, back trajectories demonstrate that air may enter the SLS from any direction, but consistent with the results from the first two frameworks, early ice melt onset and early ice retreat are both associated with a greater tendency for southerly flow. Using late ice melt years (Figure 6a) results in five clusters, one of which comes from the north. This northerly cluster is absent when using early ice melt years, and a southerly (from the south) track is present instead (Figure 6c). For ice retreat, although the northeasterly cluster is the largest regardless of composite period, 50% of trajectories belong to the more southerly clusters during early retreat years (Figure 6d), whereas only 26% do in late retreat years (Figure 6b).

3.3. Predictability

Snow retreat in the WSP is only valuable to seasonal predictions of ice melt onset and ice retreat in the SLS if it adds predictive skill to alternative models, such as concurrent SIC in the SLS and/or atmospheric variables over the SLS. Models for which sea ice melt onset in the SLS is the left-hand variable are shown in Table 3. Of all 8,191 possible models with only atmospheric variables, the lowest BIC results from a simple model with just 2-m temperature (t2m). About 20% of the variance in melt onset in the SLS, which occurs in June, can be explained by the 2-m temperature during the 10 April to 9 May period. This is about the same amount of

Table 2
Correlation of Atmospheric Variables Averaged for the Southern Laptev Sea Region (Figure 1) With Detrended Snow Retreat in the West Siberian Plain

Period day of year dates	Snow cover retreat 100 to 129 10 April to 9 May	Sea ice melt onset 153 to 182 2 June to 1 July	Sea ice retreat 193 to 222 12 July to 10 August
Temperature (2 m)	−0.16 (0.37)	−0.40 (0.02)	−0.59 (<0.01)
Temperature (925 hPa)	−0.19 (0.27)	−0.41 (0.01)	−0.48 (<0.01)
Temperature advection (925 hPa)	−0.10 (0.56)	−0.46 (<0.01)	−0.15 (0.37)
Total column water vapor	−0.31 (0.07)	−0.32 (0.05)	−0.40 (0.01)
Downwelling longwave radiation	−0.19 (0.28)	−0.39 (0.02)	−0.49 (<0.01)
Downwelling shortwave radiation	+0.06 (0.74)	+0.30 (0.07)	+0.18 (0.29)
Sensible heat flux	−0.17 (0.32)	+0.09 (0.62)	−0.00 (0.98)
Latent heat flux	−0.24 (0.16)	+0.18 (0.28)	−0.08 (0.65)
Meridional wind (925 hPa)	+0.11 (0.50)	−0.33 (0.04)	−0.38 (0.02)

Note. Atmospheric variables are temporally averaged for three different periods. Because of significant linear trends in downwelling longwave radiation and temperature, these time series are detrended first. Pearson's *r* is reported with *p*-values in parentheses. Correlations significant at the 90% confidence level are in bold.

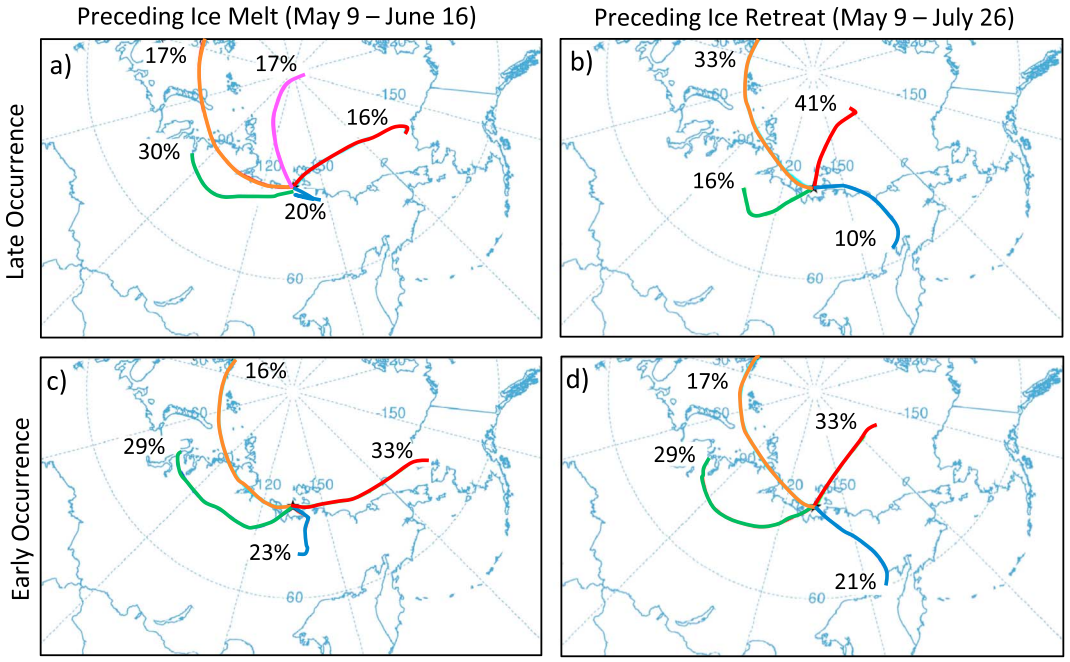

Figure 6. Clusters of eight-day back trajectories at 925 hPa from the Hybrid Single-Particle Lagrangian Integrated Trajectory (HYSPLIT) model (rounded to the nearest whole number) from the point 73°N, 135°E. Trajectories were calculated for the period (a and c) 9 May to 16 June and (b and d) 9 May to 26 July and clustered separately for (a and b) years with extreme late and (c and d) years with extreme early sea ice melt onset or retreat in the southern Laptev Sea.

explained variance as using the detrended anomaly of SIC in the SLS on 9 May. Snow retreat in the WSP, over 1,000 km away, performs better than either of those models, explaining 26% of the variance. The best possible model using any combination of variables (based on BIC) combines SIC on 9 May, WSP snow retreat (which always precedes 9 May), and the sensible heat flux over the SLS during the 10 April to 9 May period. This is about three weeks before the earliest recorded sea ice melt onset (29 May) and explains 53% of the variance in melt onset. The positive coefficient for sensible heat flux indicates that ice melt onset begins earlier if the sensible heat flux is more downward (or less upward) than normal. If sensible heat flux is omitted from consideration, 2-m temperature becomes the best third variable to include and has a negative coefficient. In other words, after controlling for WSP snow retreat and SIC, that sensible heat flux becomes a useful predictor largely because a more downward (negative) flux represents a warmer atmosphere.

Table 3
Comparison of Linear Regression Models for Which the Y Variable is the Sea Ice Melt Onset Time Series in the Southern Laptev Sea

Model description	Model results	R^2	BIC	*p*-value
1. SIC on 9 May in southern Laptev Sea	−0.03 + 0.65 * SIC	0.19	239.4	0.007
2. Lowest BIC model with only atmospheric variables	−0.09 − 1.75 * t2m	0.20	239.0	0.006
3. SCR in West Siberian Plain	0.01 + 0.44 * SCR	0.26	236.41	0.002
4. SCR + SIC	0.05 + 0.40 * SCR + 0.58 * SIC	0.41	231.50	<0.001
5. Lowest BIC model	0.07 + 0.45 * SCR + 0.67 * SIC + 0.78 * HFLUX	0.54	226.50	<0.001

Note. All time series in the models reported are detrended. Units are days for snow cover retreat (SCR) and sea ice melt onset, % for sea ice concentration (SIC), °C for 2-m temperature (t2m), and W/m^2 for the sensible heat flux (HFLUX). Figure S11a is a graph of the residuals for each model.
BIC, Bayesian Information Criterion.

Table 4
Comparison of Linear Regression Models for Which the Y Variable is the Sea Ice Retreat Time Series in the Southern Laptev Sea

Model description	Model results	R^2	BIC	*p*-value
1. SIC on 9 May in southern Laptev Sea	−0.03 + 0.89 * SIC	0.14	274.8	0.022
2. Lowest BIC model with only atmospheric variables	−0.10 + 0.08 * GPH − 3.95 * t925	0.26	273.1	0.007
3. SCR in West Siberian Plain	0.05 + 0.74 * SCR	0.29	268.1	<0.001
4. SCR + SIC	0.11 + 0.69 * SCR + 0.77 * SIC	0.40	265.6	<0.001
5. Lowest BIC model	0.03 + 0.64 * SCR + 0.07 * GPH − 3.33 * t925	0.48	264.4	<0.001

Note. All time series in the models reported are detrended except for geopotential height at 500 hPa (GPH). Units are days for snow retreat (SCR) and sea ice retreat, % for sea ice concentration (SIC), °C for 925 hPa temperature (t925), and m for GPH. Figure S11b is a graph of the residuals for each model.
BIC, Bayesian Information Criterion.

Predicting melt onset, however, has limited practical application. Though the timing of melt onset is important for melt pond formation, which in turn has predictive skill for total Arctic sea ice extent (e.g., Schröder et al., 2014), for most purposes, it is more valuable to know the timing of ice retreat. The average interval between snow retreat and sea ice retreat is 93 days (compared to 53 days for melt onset), but the predictive skill is very similar. Alone, snow cover retreat in the WSP explains 29% of the variance in sea ice retreat in the SLS, which is better than either SIC on 9 May or the best atmospheric model using the 10 April to 9 May average period. Using both snow retreat and SIC yields a slightly better model based on BIC and explains 40% of the variance. This is very similar to predicting sea ice melt onset. Finally, the overall lowest BIC of any possible model includes a combination of WSP snow retreat and both temperature at 925 hPa (t925) and GPH at 500 hPa over the SLS. The coefficients indicate that earlier sea ice retreat can be expected when snow retreat is earlier, temperature is higher, and 500-hPa heights are slightly lower. As with sea ice melt onset, despite spatial separation, WSP snow retreat is a valuable predictor of sea ice retreat in the SLS when compared to other potential predictors with a similar time lag.

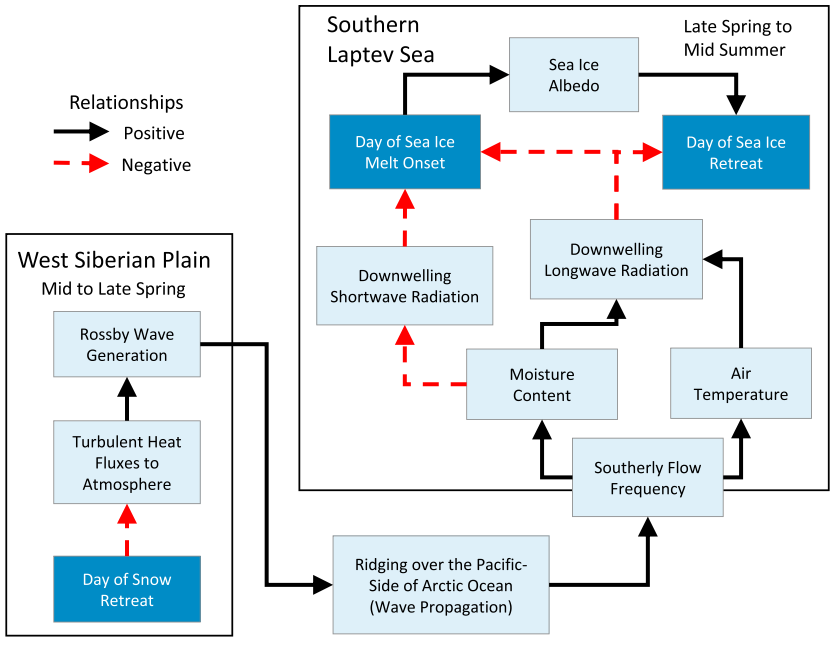

Figure 7. Schematic diagram showing relationships relevant to how variability in West Siberian Plain (WSP) snow cover retreat impacts subsequent sea ice melt onset and retreat in the southern Laptev Sea (SLS).

4. Discussion and Conclusions

4.1. Statistical Links and Predictability

Of the three research questions posed, the answer to the first is the most straightforward: Significant statistical links exist between melt onset and sea ice retreat in the SLS and retreat of the snow cover in the WSP. Notably, although ice retreat in the SLS has greater variance than ice melt onset and a longer time gap between it and WSP snow retreat, its correlation with WSP snow retreat is slightly larger. Addressing the third research question, the timing of snow retreat in the WSP has the potential to improve forecasts of sea ice retreat in the SLS at a lead time of up to about three months, which may be of use to shipping operations and other activities. As shown in Tables 3 and 4, WSP snow retreat alone outperforms models that use either atmospheric parameters or SIC within the SLS. Comparing all 32,707 possible statistical models, the lowest BIC model included snow retreat in the WSP, whether predicting sea ice melt onset or retreat in the SLS.

That said, detrended snow retreat day improves predictions only incrementally. Alone, it explains 26 and 29% of the detrended variance in sea ice melt onset and retreat, respectively. This level of predictive skill at the beginning of May compares well to several other predictions of summer sea ice conditions (e.g., Schröder et al., 2014; Petty et al., 2017), including regional predictions of the SLS ice extent using a coupled atmosphere-ocean-sea ice-land model (e.g., Bushuk et al., 2017). However, it is notably lower than predictions of sea ice retreat made for the Chukchi Sea based solely on heat inflow through the Bering Strait (Serreze et al., 2016). Combined with other parameters, the greatest explained variance in any model is 53 and 48% for ice melt onset and ice retreat, respectively. Additionally, the snow record has a coarse weekly temporal resolution. Daily satellite products of snow cover are available (National Ice Center, 2008; http://nsidc.org/data/G02156), but the continuous record is relatively short (1998 to present). The relationships also may not all be linear, as assumed in the regression models.

4.2. The Atmospheric Pathway

Although statistical utility of the snow-sea ice connection is the motivation for this study, understanding the relationship is incomplete without a clear physical explanation. As shown in Figure 3, especially early WSP snow retreat is typically followed by periods of especially warm, moist conditions over the SLS that increase downwelling longwave radiation while reducing downwelling shortwave. Previous studies have shown that such atmospheric conditions lead to early sea ice melt onset throughout the Arctic Ocean (Kapsch et al., 2016; Liu & Schweiger, 2017; Mortin et al., 2016). These atmospheric anomalies coincide with more frequent winds from the south (Figures 3k and 3l), which, based on back trajectory analysis (Figure 6), also precede especially early sea ice melt onset and retreat in the SLS. Rather than a direct relationship whereby air masses modified over the WSP subsequently impact the SLS, these results suggest an indirect relationship whereby snow retreat variability in the WSP impacts where the air masses moving over the SLS originate.

One possible explanation for why this relationship exists is that the correlations result from a common cause: all events occur earlier or later than normal because the wider region of the Siberian Arctic experiences warmer/wetter or cooler/drier conditions, respectively. The variability of snow retreat has no real impact on sea ice melt onset and retreat; the atmosphere is a confounding variable. In the purest version of this scenario, we would expect the atmospheric anomalies that induce early or late snow retreat over the WSP to persist into the later periods. Figure 3 demonstrates that this is not the case. In both regions of interest, the atmospheric response to snow retreat variability has distinct signatures in the periods during and after snow retreat.

A more likely possibility is that variability in WSP snow retreat has some physical effect on regional atmospheric circulation. More precisely, and consistent with both Matsumura et al. (2010) and Xu and Dirmeyer (2011), early snow retreat from the WSP leads to an albedo feedback, locally higher temperatures, and greater sensible and latent heat fluxes to the atmosphere (Figure 4). These local effects are only apparent in spring, disappearing by summer, but they set in motion a circulation response through the generation of Rossby waves (Figure 5) that propagate eastward (Figure 3). In this way, early snow retreat in the WSP encourages a summer circulation pattern with more ridging over the Kolyma Lowland and East Siberian Sea and troughing over the Taymyr Peninsula and Kara Sea. Impacts on circulation persist through summer and are similar to the findings of Matsumura and Yamazaki (2012) and Matsumura et al. (2014), although their work focused on

a larger spatial scale. These relationships could be further tested in a future effort using a coupled atmospheric-ocean-ice model.

Matsumura et al. (2014) also observed a negative AO-like pattern in response to less Eurasian snow cover, warmer temperatures over the Arctic Ocean, and lower September SIC, especially on the Eurasian side of the Arctic Ocean. The snow retreat time series used here represents a smaller area, but weak positive correlations between WSP snow retreat and the monthly AO index (Figure S12) in both June ($r = 0.33$, $p = 0.05$) and July ($r = 0.28$, $p = 0.09$) are generally consistent with their results. Later WSP snow retreat is commonly followed by positive AO conditions in summer; early snow retreat is commonly followed by negative AO conditions. Conversely, that in spring, positive AO conditions often precede low snow cover extents (Matsumura et al., 2014). Consistent with this relationship, the best model for predicting sea ice retreat in the SLS includes a positive coefficient for 500-hPa height measured over the SLS from 10 April to 9 May. This indicates lower heights in the spring, which are characteristic of positive AO conditions. The correlation between the April AO index and WSP snow retreat is also consistent with this pattern but not significant ($r = -0.24$, $p = 0.16$).

Although not conclusive proof of cause and effect, the results presented here support the following model of the links within this system (Figure 7). In late April, snow retreats from the WSP. If that retreat occurs especially early (by 11 to 21 days), surface-atmosphere interactions and atmospheric wave generation are enhanced. Propagation of these waves leads to ridging over the Arctic Ocean, especially the Pacific side. This encourages southerly flow over the SLS, which brings warmer, moister air, which enhances downwelling longwave radiation. This in turn encourages earlier melt onset and retreat for sea ice. Additionally, earlier melt onset means a quicker decline in sea ice albedo, which further encourages early sea ice retreat (Perovich & Polashenski, 2012; Petty et al., 2017; Schröder et al., 2014). Therefore, even if other sources of variability disrupt the circulation patterns encouraged by earlier WSP snow retreat, earlier sea ice melt onset reinforces the nudging of sea ice toward earlier retreat. Through these several physical links, anomalies in WSP snow retreat are echoed in sea ice retreat in the SLS three months later.

Acknowledgments
This work was supported by NOAA grant NA15OAR4310171 and NSF grants PLR 1603914 and OPP 1748953. We thank three anonymous reviewers for their constructive comments and acknowledge the contributions of the late Drew Slater. Sea ice and snow retreat day data are available at ftp://sidads.colorado.edu/pub/projects/SIPN under subdirectories Retreat_Advance and Snow_retreat2, respectively.

References

Bracken, C., Rajagopalan, B., Alexander, M., & Gangopadhyay, S. (2015). Spatial variability of seasonal extreme precipitation in the western United States. *Journal of Geophysical Research: Atmospheres*, *120*, 4522–4533. https://doi.org/10.1002/2015JD023205

Brodzik, M. J., & Armstrong, R. (2013). *Northern Hemisphere EASE-Grid 2.0 weekly snow cover and sea ice extent, Version 4*, (pp. 1979–2014). Boulder, Colorado USA: NASA National Snow and Ice Data Center Distributed Active Archive Center. https://doi.org/10.5067/P7O0HGJLYUQU. Accessed 25 April 2017

Bushuk, M., Msadek, R., Winton, M., Vecchi, G. A., Gudgel, R., Rosati, A., & Yang, X. (2017). Skillful regional prediction of Arctic sea ice on seasonal timescales. *Geophysical Research Letters*, *44*, 4953–4964. https://doi.org/10.1002/2017GL073155

Cavalieri, D. J., Parkinson, C. L., Gloersen, P., & Zwally, H. J. (1996, updated yearly). *Sea Ice Concentrations from Nimbus-7 SMMR and DMSP SSM/I-SSMIS passive microwave data, Version 1* (pp. 1979–2014). Boulder, Colorado USA: NASA National Snow and Ice Data Center Distributed Active Archive Center. https://doi.org/10.5067/8GQ8LZQVL0VL. Accessed 25 April 2017

Clark, M. P., & Serreze, M. C. (2000). Effects of variations in East Asian snow cover on modulating atmospheric circulation over the North Pacific Ocean. *Journal of Climate*, *13*(20), 3700–3710. https://doi.org/10.1175/1520-0442(2000)013<3700:EOVIEA>2.0.CO;2

Draxler, R., Stunder, B., Rolph, G., Stein, A., & Taylor, A. (2016). HYSPLIT4 user's guide. Retrieved December 14, 2017 from https://www.arl.noaa.gov/documents/reports/hysplit_user_guide.pdf

Draxler, R. R. (1999). HYSPLIT_4 user's guide, NOAA Technical Memorandum ERL ARL-230, June, 35 pp.

Draxler, R. R., & Hess, G. D. (1997). Description of the HYSPLIT_4 modeling system, NOAA Technical Memorandum ERL ARL-224, 24 pp.

Draxler, R. R., & Hess, G. D. (1998). An overview of the HYSPLIT_4 modelling system for trajectories, dispersion, and deposition. *Australian Meteorological Magazine*, *47*, 295–308.

Edmon, H. J. Jr., Hoskins, B. J., & McIntyre, M. E. (1980). Eliassen-Palm cross sections for the troposphere. *Journal of the Atmospheric Sciences*, *37*(12), 2600–2616. https://doi.org/10.1175/1520-0469(1980)037<2600:EPCSFT>2.0.CO;2

García-Herrera, R., & Barriopedro, D. (2006). Northern Hemisphere snow cover and atmospheric blocking variability. *Journal of Geophysical Research*, *111*, D21104. https://doi.org/10.1029/2005JD006975

Gelaro, R., McCarty, W., Suárez, M. J., Todling, R., Molod, A., Takacs, L., et al. (2017). The Modern-Era Retrospective Analysis for Research and Applications, Version 2 (MERRA-2). *Journal of Climate*, *30*(14), 5419–5454. https://doi.org/10.1175/JCLI-D-16-0758.1

Gong, G., Cohen, J., Entekhabi, D., & Ge, Y. (2007). Hemispheric-scale climate response to Northern Eurasia land surface characteristics and snow anomalies. *Global and Planetary Change*, *56*(3–4), 359–370. https://doi.org/10.1016/j.gloplacha.2006.07.025

Gustafsson, M., Rayner, D., & Chen, D. (2010). Extreme rainfall events in southern Sweden: Where does the moisture come from? *Tellus A: Dynamic Meteorology and Oceanography*, *62*(5), 605–616, http://doi.org/10.1111/j.1600-0870.2010.00456.x

Hamilton, L. C., & Stroeve, J. (2016). 400 predictions: The SEARCH Sea Ice Outlook 2008–2015. *Polar Geography*, *39*, 274–287.

Helfrich, S. R., McNamara, D., Ramsay, B. H., Baldwin, T., & Kasheta, T. (2007). Enhancements to, and forthcoming developments in the Interactive Multisensor Snow and Ice Mapping System (IMS). *Hydrological Processes*, *21*(12), 1576–1586. https://doi.org/10.1002/hyp.6720

Holland, M. M., & Stroeve, J. C. (2011). Changing seasonal sea ice predictor relationships in a changing Arctic climate. *Geophysical Research Letters*, *38*, L18501. https://doi.org/10.1029/2011GL049303

Jahn, A., Kay, J. E., Holland, M. M., & Hall, D. M. (2016). How predictable is the timing of a summer ice-free Arctic? *Geophysical Research Letters*, *43*, 9113–9120. https://doi.org/10.1002/2016GL070067

Kalnay, E., Kanamitsu, M., & Kistler, R. (1996). The NCEP/NCAR 40-Year Reanalysis Project. *Bulletin of the American Meteorological Society*, *77*(3), 437–471. https://doi.org/10.1175/1520-0477(1996)077<0437:TNYRP>2.0.CO;2

Kapsch, M.-L., Graversen, R. G., & Tjernstrom, M. (2013). Springtime atmospheric energy transport and the control of Arctic summer sea–ice extent. *Nature Climate Change*, *3*(8), 744–748. https://doi.org/10.1038/nclimate1884

Kapsch, M.-L., Graversen, R. G., Tjernström, M., & Bintanja, R. (2016). The effect of downwelling longwave and shortwave radiation on Arctic summer sea ice. *Journal of Climate*, *29*(3), 1143–1159. https://doi.org/10.1175/JCLI-D-15-0238.1

Kumar, A., & Yang, F. (2003). Comparative influence of snow and SST variability on extratropical climate in Northern winter. *Journal of Climate*, *16*(13), 2248–2261. https://doi.org/10.1175/2771.1

Lahn, G., & Emmerson, C. (2012). Arctic opening: Opportunity and risk in the High North, Chatham House-Lloyd's Risk Insight Report, 60 pp.

Liu, Z., & Schweiger, A. (2017). Synoptic conditions, clouds, and sea ice melt-onset in the Beaufort and Chukchi Seasonal Ice Zone. *Journal of Climate*, *30*(17), 6999–7016. https://doi.org/10.1175/JCLI-D-16-0887.1

Markus, T., Stroeve, J. C., & Miller, J. (2009). Recent changes in Arctic sea ice melt onset, freezeup, and melt season length. *Journal of Geophysical Research*, *114*, C12024. https://doi.org/10.1029/2009JC005436

Matsumura, S., & Yamazaki, K. (2012). Eurasian subarctic summer climate in response to anomalous snow cover. *Journal of Climate*, *25*(4), 1305–1317. https://doi.org/10.1175/2011JCLI4116.1

Matsumura, S., Yamazaki, K., & Tokioka, T. (2010). Summertime land-atmosphere interactions in response to anomalous springtime snow cover in northern Eurasia. *Journal of Geophysical Research*, *115*, D20107. https://doi.org/10.1029/2009JD012342

Matsumura, S., Zhang, X., & Yamazaki, K. (2014). Summer Arctic atmospheric circulation response to spring Eurasian snow cover and its possible linkage to accelerated sea ice decrease. *Journal of Climate*, *27*(17), 6551–6558. https://doi.org/10.1175/JCLI-D-13-00549.1

Metzger, E. J., Helber, R. W., Hogan, P. J., Posey, P. G., Thoppil, P. G., Townsend, T. L., et al. (2017). *Global Ocean Forecast System 3.1 validation test (No. AD1034517)*, (pp. 1–60). Stennis Space Center, USA: Naval Research Lab.

Metzger, R., Smedstad, O., Thoppil, P., Hurlburt, H., Cummings, J., Wallcraft, A., et al. (2014). US Navy operational global ocean and Arctic ice prediction systems. *Oceanography*, *27*(3), 32–43. https://doi.org/10.5670/oceanog.2014.66

Moon, Y.-I., Rajagopalan, B., & Lall, U. (1995). Estimation of mutual information using kernel density estimators. *Physical Review E*, *52*(3), 2318–2321. https://doi.org/10.1103/PhysRevE.52.2318

Mortin, J., Svensson, G., Graversen, R. G., Kapsch, M.-L., Stroeve, J. C., & Boisvert, L. N. (2016). Melt onset over Arctic sea ice controlled by atmospheric moisture transport. *Geophysical Research Letters*, *43*, 6636–6642. https://doi.org/10.1002/2016GL069330

National Ice Center (2008, updated daily). *IMS Daily Northern Hemisphere Snow and Ice Analysis at 1 km, 4 km, and 24 km Resolutions, Version 1*. Boulder, Colorado USA: NSIDC: National Snow and Ice Data Center. https://doi.org/10.7265/N52R3PMC

Notz, D., & Stroeve, J. (2016). Observed Arctic sea-ice loss directly follows anthropogenic CO_2 emission. *Science*, *354*(6313), 747–750. https://doi.org/10.1126/science.aag2345

Ogi, M., & Wallace, J. M. (2007). Summer minimum Arctic sea ice extent and the associated summer atmospheric circulation. *Geophysical Research Letters* , *34*, L12705. https://doi.org/10.1029/2007GL029897

Orsolini, Y. J., & Kvamstø, N. G. (2009). Role of Eurasian snow cover in wintertime circulation: Decadal simulations forced with satellite observations. *Journal of Geophysical Research*, *114*, D19108. https://doi.org/10.1029/2009JD012253

Overland, J. E., & Wang, M. (2013). When will the summer Arctic be nearly sea-ice free? *Geophysical Research Letters*, *40*, 2097–2101. https://doi.org/10.1002/grl.50316

Peings, Y., Douville, H., Alkama, R., & Decharme, B. (2011). Snow contribution to springtime atmospheric predictability over the second half of the twentieth century. *Climate Dynamics*, *37*, 985–1004. https://doi.org/10.1007/s00382-010-0884-1

Petty, A. A., Schröder, D., Stroeve, J. C., Markus, T., Miller, J., Kurtz, N. T., et al. (2017). Skillful spring forecasts of September Arctic sea ice extent using passive microwave sea ice observations. *Earth's Future*, *5*, 254–263. https://doi.org/10.1002/2016EF000495

Perovich, D. K., & Polashenski, C. (2012). Albedo evolution of seasonal Arctic sea ice. *Geophysical Research Letters*, *39*, L08501. https://doi.org/10.1029/2012GL051432

Rigor, I. G., Wallace, J. M., & Colony, R. L. (2002). Response of sea ice to the Arctic Oscillation. *Journal of Climate*, *15*(18), 2648–2663. https://doi.org/10.1175/1520-0442(2002)015<2648:ROSITT>2.0.CO;2

Robinson, D. (2012). *NOAA/NCDC Climate Data Record (CDR) of Northern Hemisphere (NH) snow cover extent (SCE). 1979–2014*. New Jersey, USA: Rutgers University Global Snow Lab.

Schlichtholz, P. (2011). Influence of oceanic heat variability on sea ice anomalies in the Nordic seas. *Geophysical Research Letters*, *38*, L05705. https://doi.org/10.1029/2010GL045894

Schröder, D., Feltham, D. L., Flocco, D., & Tsamados, M. (2014). September Arctic sea-ice minimum predicted by spring melt-pond fraction. *Nature Climate Change*, *4*(5), 353–357. https://doi.org/10.1038/nclimate2203

Schwarz, G. (1978). Estimating the dimension of a model. *The Annals of Statistics*, *6*(2), 461–464. https://doi.org/10.1214/aos/1176344136

Serreze, M. C., Crawford, A. D., Stroeve, J. C., Barrett, A. P., & Woodgate, R. A. (2016). Variability, trends, and predictability of seasonal sea ice retreat and advance in the Chukchi Sea. *Journal of Geophysical Research: Oceans*, *127*, 7308–7325. https://doi.org/10.1002/2016JC011977

Stammerjohn, S., Massom, R., Rind, D., & Martinson, D. (2012). Regions of rapid sea ice change: An inter-hemispheric seasonal comparison. *Geophysical Research Letters*, *39*, L06501. https://doi.org/10.1029/2012GL050874

Stroeve, J., Blanchard-Wrigglesworth, E., Guemas, V., Howell, S. E. L., Massonnet, F., & Tietsche, S. (2015). Improving predictions of Arctic sea ice extent. *Eos*, *96*. https://doi.org/10.1029/2015EO031431

Stroeve, J. C., Crawford, A. D., & Stammerjohn, S. (2016). Using timing of ice retreat to predict timing of fall freeze-up in the Arctic. *Geophysical Research Letters*, *43*, 6332–6340. https://doi.org/10.1002/2016GL069314

Stroeve, J. C., Hamilton, L. C., Bitz, C. M., & Blanchard-Wrigglesworth, E. (2014). Predicting September sea ice: Ensemble skill of the SEARCH Sea Ice Outlook 2008–2013. *Geophysical Research Letters*, *41*, 2411–2418. https://doi.org/10.1002/2014GL059388

Stroeve, J. C., Holland, M. M., & Meier, W. (2007). Arctic sea ice decline: Faster than forecast. *Geophysical Research Letters*, *34*, L09501. https://doi.org/10.1029/2007GL029703

Stroeve, J. C., Kattsov, V., Barrett, A., Serreze, M. C., Pavlova, T., Holland, M. M., & Meier, W. N. (2012). Trends in Arctic sea ice extent from CMIP5, CMIP3 and observations. *Geophysical Research Letters*, *39*, L16502. https://doi.org/10.1029/2012GL052676

Stroeve, J. C., Markus, T., Bosivert, L., Miller, J., & Barrett, A. (2014). Changes in Arctic melt season and implications for sea ice loss. *Geophysical Research Letters*, *41*, 1216–1225. https://doi.org/10.1002/2013GL058951

Stroeve, J. C., Serreze, M. C., Holland, M. M., Kay, J. E., Maslanik, J. A., & Barrett, A. P. (2012). The Arctic's rapidly shrinking sea ice cover: A research synthesis. *Climatic Change*, *110*(3–4), 1005–1027. https://doi.org/10.1007/s10584-011-0101-1

Takaya, K., & Nakamura, H. (2001). A formulation of a phase-independent wave-activity flux for stationary and migratory quasigeostrophic eddies on a zonally varying basic flow. *Journal of Atmospheric Sciences*, *58*, 608–627.

Thompson, D. W. J., & Wallace, J. M. (1998). The Arctic Oscillation signature in the wintertime geopotential height and temperature fields. *Geophysical Research Letters*, *25*(9), 1297–1300. https://doi.org/10.1029/98GL00950

Wegmann, M., Orsolini, Y., Vázquez, M., Gimeno, L., Nieto, R., Bulygina, O., et al. (2015). Arctic moisture source for Eurasian snow cover variations in autumn. *Environmental Research Letters*, *10*(5), 054015. https://doi.org/10.1088/1748-9326/10/5/054015

Williams, J., Tremblay, B., Newton, R., & Allard, R. (2016). Dynamic preconditioning of the minimum September sea-ice extent. *Journal of Climate*, *29*(16), 5879–5891. https://doi.org/10.1175/JCLI-D-15-0515.1

Woodgate, R. A., Stafford, K. M., & Prahl, F. G. (2015). A synthesis of year-round interdisciplinary mooring measurements in the Bering Strait (1990–2014) and the RUSALCA years (2004–2011). *Oceanography*, *28*, 46–67. https://doi.org/10.5670/oceanog.2015.57

Woodgate, R. A., Weingartner, T., & Lindsay, R. (2010). The 2007 Bering Strait oceanic heat flux and anomalous Arctic sea-ice retreat. *Geophysical Research Letters*, *37*, L01602. https://doi.org/10.1029/2009GL041621

Xu, L., & Dirmeyer, P. (2011). Snow-atmosphere coupling strength in a global atmospheric model. *Geophysical Research Letters*, *38*, L13401. https://doi.org/10.1029/2011GL048049